Supporting Information

Selective photocatalytic CO_2 reduction in water through anchoring of a molecular Ni catalyst on CdS nanocrystals

Moritz F. Kuehnel,[‡] Katherine L. Orchard,[‡] Kristian E. Dalle and Erwin Reisner*

Christian Doppler Laboratory for Sustainable SynGas Chemistry,
Department of Chemistry, University of Cambridge,
Lensfield Road, CB2 1EW, Cambridge, UK.

*Corresponding author email address: reisner@ch.cam.ac.uk

Experimental Section

Materials. All chemicals were obtained from commercial sources in the highest available purities and used as received. $Ni(BF_4)_2 \times 6H_2O$ (99%) was purchased from Acros Organics, $Zn(BF_4)_2 \times H_2O$ (18% Zn min) and 2,2':6',2''-terpyridine (terpy, 97%) were purchased from Alfa Aesar, 2,2':6',2''-terpyridine-4'-carboxylic acid (terpyC, 98%), 2,2':6',2''-terpyridine-4'-phosphonic acid (terpyP, 98%) and 2,2':6',2''-terpyridine-4'-thiol (terpyS, 98%) were purchased form HetCat, Switzerland. $Fe(BF_4)_2 \times 6H_2O$ (97%), triethanolamine (TEOA, ≥99.5%), CdO (99.998%), sulfur (99.998%), oleic acid (OA, 90%), octadecene (ODE, 90%), 3-mercaptopropionic acid (MPA, ≥99 %), tetramethylammonium hydroxide pentahydrate (TMAOH, 99 %), triethyloxonium tetrafluoroborate (1.0 M in dichloromethane) and trimethyloxonium tetrafluoroborate (96 %) were purchased from Sigma-Aldrich. Anhydrous solvents were purchased from Acros Organics with the following purities: $CHCl_3$ (99.9 %), *N*,*N*-dimethylformamide (DMF, 99.8%), acetonitrile (ACN, 99.9 %). All other organic solvents used were HPLC grade. All aqueous experimental solutions were prepared with distilled water and all aqueous analytical samples were prepared with ultrapure water (DI water; Milli-Q®, 18.2 MΩ cm). $^{13}CO_2$ (>99 atom% ^{13}C) was purchased from Sigma Aldrich. $Ni(terpy_2)(PF_6)_2$ was prepared by a literature procedure.[1]

CdS QD Preparation. CdS QDs with different surface functionalities ($CdS\text{-}BF_4$) were prepared by either ligand stripping ($QD\text{-}BF_4$) or ligand exchange (QD-MPA) of oleic acid-capped QDs (QD-OA) as previously reported.[2] To ensure that all QDs had a comparable absorption maximum, larger QD-OA particles (λ_{max} = 466 nm, D = 6.0±0.9 nm) were used as the starting material for $QD\text{-}BF_4$ compared to those used for QD-MPA (λ_{max} = 443 nm, D = 4.4±0.4 nm) in order to compensate for the known etching of the particles during ligand stripping.[2]

QD-OA. Oleic-acid capped QDs were prepared by modified literature procedures.[3] Briefly, sulfur (0.08 g) in ODE (30 g) was added to a solution of CdO (0.64 g) and OA (26 g) in ODE (70 g), held at 280°C. The solution was allowed to cool to 250°C and was maintained at this temperature for 120 s before quenching by rapid cooling. QD-OA with λ_{max} = 443 nm were obtained by adding the sulfur solution rapidly whereas QD-OA with λ_{max} = 466 nm were obtained by adding half of the sulfur solution rapidly and adding the remaining solution dropwise over 120 s; the total time at 250°C was 120 s for both types of QD (i.e. the solution was quenched immediately after the final addition of sulfur solution for $QD\text{-}OA_{466}$). The particles were precipitated from 1:1 hexane:methanol using excess acetone, centrifuged at 7000 rpm for 3 min, and re-dispersed in hexane. Two further washing steps were carried out using hexane and acetone as solvent and non-solvent, respectively, before finally dispersing in hexane (20 mL).

$QD\text{-}BF_4$. Ligand free particles were prepared under inert atmosphere by a modified literature procedure.[4] Briefly, $QD\text{-}OA_{466}$ solution (5 mL in hexane) was reduced to dryness and redispersed in a mixture of anhydrous $CHCl_3$ (15 mL) and anhydrous DMF (1.6 mL). Triethyloxonium tetrafluoroborate solution (20 mL) was added and stirred for 1 h. Aliquots of trimethyloxonium tetrafluoroborate solution (1.0 M in ACN, 1.6 mL total solution) were added until the particles precipitated. The stripped particles were centrifuged (7000 rpm, 3 min), dried in air for 1 min, and re-dispersed in DMF (2 mL).

QD-MPA. Ligand exchange with MPA was carried out according to a literature procedure.[5] MPA (0.5 mL) was dispersed in 1:1 chloroform:methanol (10 mL) and the pH adjusted to 11 with TMAOH. QD-OA_{443} solution (2 mL) was added to this mixture and stirred in the dark for at least 16 h. The QDs were precipitated with excess acetone and centrifuged (7000 rpm, 3 min). The isolated particles were washed with acetone before being dispersed in water (1 mL).

QD concentration determination. The concentration of CdS (in moles of particles) was estimated from the UV absorption spectrum using the method developed by Peng and co-workers.[6] The average particle diameter, *D*, was determined from the wavelength of the first absorption maximum, λ, and the concentration of particles was determined from the absorbance at the wavelength of the first absorption maximum using the Beer-Lambert law, and an extinction coefficient, ϵ.

$$D = (-6.6521 \times 10^{-8})\lambda^3 + (1.9557 \times 10^{-4})\lambda^2 - (9.2352 \times 10^{-2})\lambda + (13.29)$$

$$\epsilon = 5500\, \Delta E\, (D)^{2.5}$$

The concentration estimated from the UV-vis spectrum was supported by Cd concentration measured by ICP-OES.

Determination of QD conduction band edge. A QD-BF_4 stock solution (4 µL) was drop-cast onto a polished glassy carbon electrode and dried *in vacuo* for 30 min. A linear sweep voltammogram of the modified electrode was subsequently recorded in aqueous solution (0.1 M TEOA, 0.1 M KCl, pH adjusted to 6.7 to match conditions during photocatalysis; Ag/AgCl reference, Pt mesh counter electrode, v = 0.1 V s^{-1}).[7]

$[Ni(terpyS)_2][PF_6]_2$. For additional characterization, $[Ni(terpyS)_2][PF_6]_2$ was synthesized by refluxing $NiCl_2{\times}6H_2O$ (31.2 mg, 0.131 mmol) and terpyS (71.2 mg, 0.268 mmol) in 1:1 ethanol/water (10 mL) under N_2. After 4 h, the solution was cooled to room temperature, filtered and saturated NH_4PF_6 in ethanol/water was added dropwise to precipitate $[Ni(terpyS)_2][PF_6]_2$. The precipitate was collected by filtration, washed with ethanol/water and dried in vacuo. Yield: 49.0 mg (43%). Analysis calculated for $[Ni(terpyS)_2][PF_6]_2{\times}0.5EtOH$: C, 41.26; H, 2.79; N, 9.31. Found: C, 41.61; H, 2.49; N, 9.48.

Quantification of released terpyS ligand during photocatalysis. Photocatalysis experiments were performed with CdS-$[Ni(terpyS)_2]^{2+}$ under standard condition but with added $Fe(BF_4)_2{\times}6H_2O$ (100 µM). The absorption peak at 578 nm was used to determine the concentration of formed $[Fe(terpyS)_2]^{2+}$, based on a calibration recorded with $[Fe(terpyS)_2]^{2+}$ assembled from $Fe(BF_4)_2{\times}6H_2O$ and two equivalents of terpyS at different concentrations in 0.1 M aq. TEOA pH 6.7 under CO_2.

Photocatalysis regeneration experiment. Photocatalysis samples were prepared as above and irradiated for 20 h. A solution of $[Ni(terpyS)_2]^{2+}$ (200 µL, 1 mM in 0.1 M aqueous TEOA, purged with 2% CH_4 in CO_2) was injected through the rubber septum and irradiation was continued for a further 7 h. Alternatively, a solution of $Ni(BF_4)_2{\times}6H_2O$ (200 µL, 1 mM in 0.1 M aqueous TEOA, purged with 2% CH_4 in CO_2) was injected after CO production had ceased and irradiation was continued.

External Quantum Efficiency (EQE). Photocatalysis samples were prepared as above, but using an air-tight, flat-sided quartz cuvette (1 cm path length) as the photoreactor. The cuvette was purged with CO_2/CH_4 (2%) and irradiated (λ = 400±5 nm, I = 1.55 mW cm^{-2}) using a LOT Quantum Design

MSH-300 monochromator and aliquots of headspace gas were taken at 3, 4, 5 and 6 h of irradiation. The EQE was calculated according to equation (1).

$$\mathrm{EQE} = \frac{2n_{CO} \times N_A \times h \times c}{t_{\mathrm{irr}} \times \lambda \times I \times A} \times 100\ \% \qquad (1)$$

Where n_{CO} is the amount of produced CO, N_A is Avogadro's constant, h is the Planck constant, c is the speed of light, t_{irr} is the irradiation time, λ is the irradiation wavelength, I is the irradiation intensity and A is the irradiated area (0.25 cm^2).

Gas Chromatography Analysis. Gas chromatography was carried out on an Agilent 7890A gas chromatograph kept at 45°C using a thermal conductivity detector (TCD). H_2 was analyzed using a HP-5 column (0.32 mm diameter) using N_2 as carrier gas at 3 mL min^{-1}. CO was analyzed using a HP-PLOT/Q column (0.53 mm diameter) attached to a HP-5 column (0.32 mm diameter) using He as carrier gas at 2 mL min^{-1}. Methane (2% CH_4 in CO_2) was used as internal standard after calibration with different mixtures of known $CH_4/H_2/CO$ compositions.

Ion Chromatography. Formic acid and oxalic acid were analyzed by ion chromatography using a Metrohm 882 compact IC plus ion chromatography system, utilizing 4 mM carbonate and 50 mL L^{-1} acetone as the eluent after calibration with solutions of different formate/oxalate concentrations.

Measurement of catalyst loading by UV-vis spectroscopy. Photocatalysis samples were prepared as described above and stirred in the dark for 30 min, either with or without purging for 10 min with CO_2. Subsequently, the particles were separated by centrifugation (10000 rpm, 3 min) and the supernatant was passed through a 2 µm syringe filter to remove residual particles. The supernatant was diluted 10-fold with 0.1 M TEOA solution and the UV-vis absorption spectrum collected. The absorption spectrum of the sample was corrected to compensate for residual CdS (based on the supernatant from an equivalent solution of QD-BF_4 without catalyst) and the quantity of catalyst remaining in the supernatant was estimated from the absorption of the corrected spectrum, based on a calibration curve for the respective catalyst at this wavelength ($[Ni(terpy)_2]^{2+}$ 320 nm, $[Ni(terpyC)_2]^{2+}$ 328 nm, $[Ni(terpyP)_2]^{2+}$ 324 nm, $[Ni(terpyS)_2]^{2+}$ 330 nm).

Inductively Coupled Plasma-Optical Emission Spectroscopy (ICP-OES). ICP-OES measurements were carried out by Mr. Christopher Rolfe (Department of Geography, University of Cambridge) using a PerkinElmer Optima 2100TM DV spectrometer. Photocatalysis samples irradiated for various times were centrifuged (7000 rpm, 3 min) and the particle pellet was separated from the supernatant. The particle precipitate was directly digested in HNO_3 (214 µL, 70% aq. solution) for 16 h before diluting to 15 mL with water. For Ni analysis, this solution was used directly; for Cd analysis, this solution was further diluted by a factor of 10. The number of catalyst molecules per quantum dot was calculated based on the measured Ni:Cd ratio, with the number of particles estimated assuming a stoichiometric Cd:S ratio and the particle diameter calculated from UV-vis spectroscopy (see QD concentration measurement, above). Error bars represent the standard deviation of two independent measurements.

Infrared Spectroscopic Analysis. FTIR spectra were recorded on a Thermo Scientific Nicolet iS50 FT-IR spectrometer. IR spectra of $[Ni(terpyS)_2]^{2+}$ and modified electrodes were recorded in ATR mode.

UV−Vis. UV−Vis spectra were recorded on a Varian Cary 50 UV−Vis spectrophotometer. Quartz glass cuvettes were used for solutions studies, FTO slides were directly mounted in the beam and measured in transmission.

Transmission electron microscopy (TEM) Transmission Electron Microscopy (TEM) images were collected using a FEI Philips Tecnai 20 instrument, with 200 kV accelerating voltage; samples were drop-cast onto holey carbon films (TAAB Laboratories Equipment Ltd).

X-ray photoelectron spectroscopy (XPS). XPS analysis was carried out at the Cambridge Microelectronics Centre on a Thermo Scientific ESCALAB Xi+ XPS Microprobe in an ultrahigh vacuum chamber. The sample was prepared by drop-casting onto a gold substrate.

Immobilization of CdS-$[Ni(terpyS)_2]^{2+}$ on electrodes. Mesoporous SnO_2 electrodes were prepared by doctor blading SnO_2 suspensions on FTO-coated glass slides (7 Ω sq^{-1}, Sigma-Aldrich) as reported previously.[8] Prior to use, electrodes were cleaned by peroxide treatment (1 h 70°C in a mixture of 100 mL water, 20 mL 30% H_2O_2 and 20 mL 35% NH_3), rinsed with water and dried at 130°C overnight. A DMF solution of QD-BF_4 (4 µL) was drop-casted on the electrode and the solvent was removed *in vacuo* overnight. The modified electrode was washed with acetonitrile and immersed in a solution of $[Ni(terpyS)_2]^{2+}$ (10 mM in acetonitrile). After 2 h, the electrode was removed from the solution, rinsed with acetonitrile and dried in air (RT, 30 min).

Treatment of data. All analytical measurements were performed in triplicate and are given as unweighted mean ± standard deviation (σ). σ of a measured value was calculated using equation (2). A minimum σ of 10 % was assumed for all experiments even where triplicate experiments gave a σ of less than 10 %.

$$\sigma = \sqrt{\frac{\sum(x-\bar{x})^2}{n-1}} \qquad (2)$$

Where n is the number of repeated measurements, x is the value of a single measurement and $\bar{x}$ is the unweighted mean of the measurements. σ was increased to 5% of $\bar{x}$ in the event that the calculated σ was below this threshold.

Supporting Figures

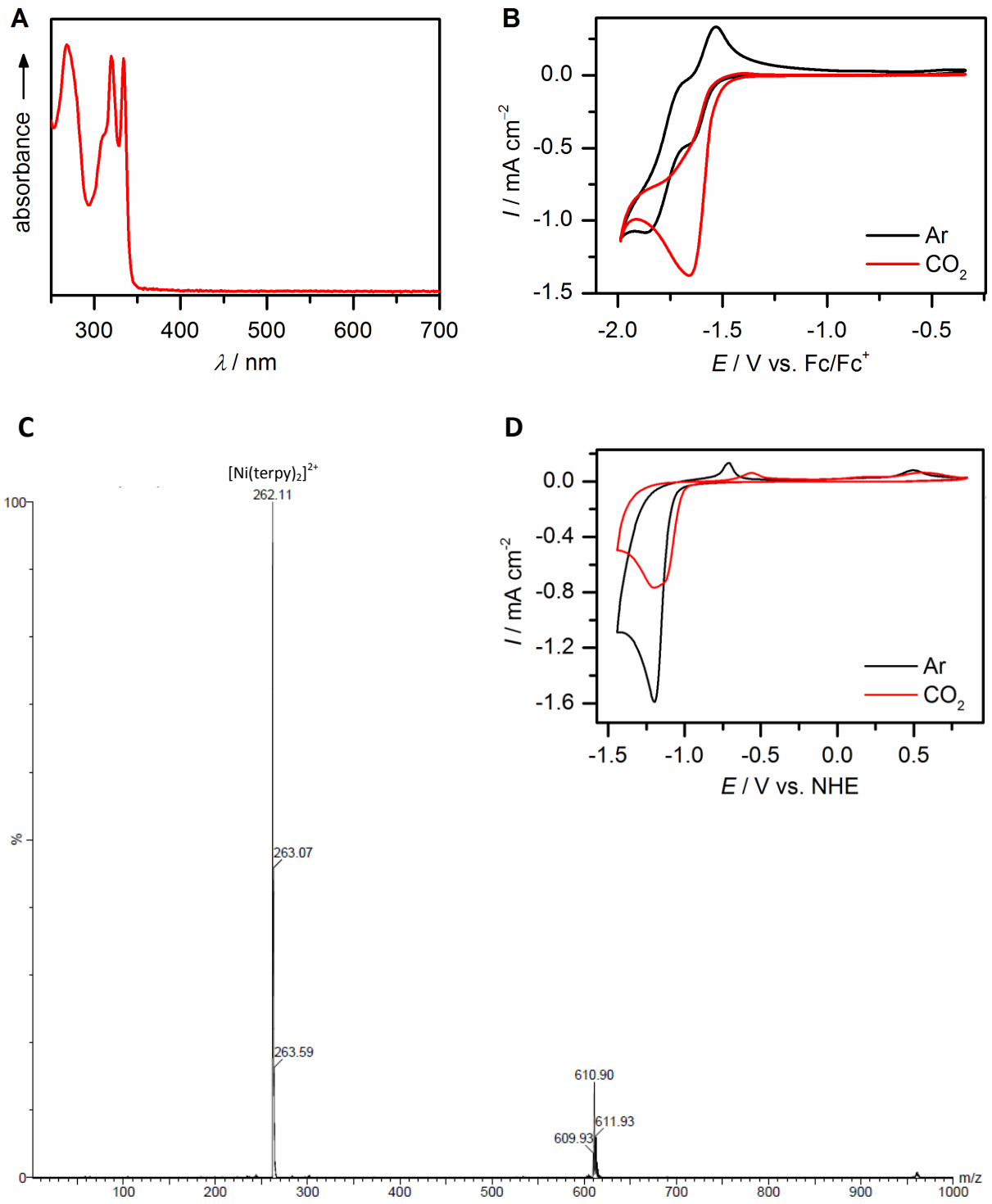

Figure S1. Characterization of self-assembled $[Ni(terpy)_2]^{2+}$. A) UV-vis spectrum in DMF solution; B) cyclic voltammogram (1.0 mM $Ni(BF_4)_2 \times 6H_2O$, 2.0 mM terpy, 0.1 M $TBABF_4$ in acetonitrile/water 3:1; v = 100 mV s^{-1}, BDD working, Pt counter, Ag/AgCl reference electrode, 25°C); C) ESI-MS spectrum in acetonitrile solution; D) cyclic voltammogram (1.0 mM $Ni(BF_4)_2 \times 6H_2O$, 2.0 mM terpy, 0.1 M TEOA, 0.1 M KCl in water/acetonitrile 19/1 v/v, pH 6.7; v = 100 mV s^{-1}, BDD working, Pt counter, Ag/AgCl reference electrode, 25°C).

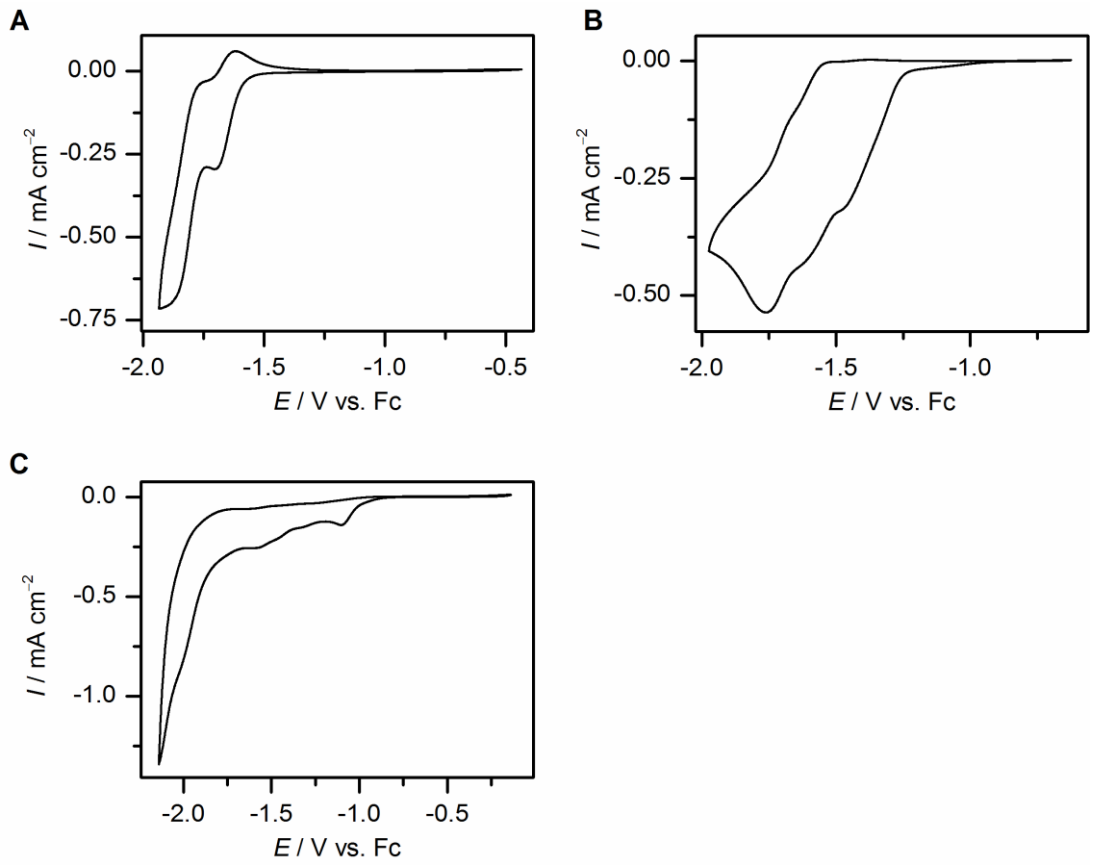

Figure S2. Cyclic voltammetry of self-assembled $[Zn(terpyX)_2]^{2+}$ complexes: A) $[Zn(terpy)_2]^{2+}$; B) $[Zn(terpyC)_2]^{2+}$; C) $[Zn(terpyS)_2]^{2+}$ (1.0 mM $Zn(BF_4)_2{\times}H_2O$, 2.0 mM terpyX, 0.1 M $TBABF_4$ in acetonitrile/water 3:1 under Ar atmosphere; v = 100 mV s^{-1}, BDD working, Pt counter, Ag/AgCl reference electrode, 25°C).

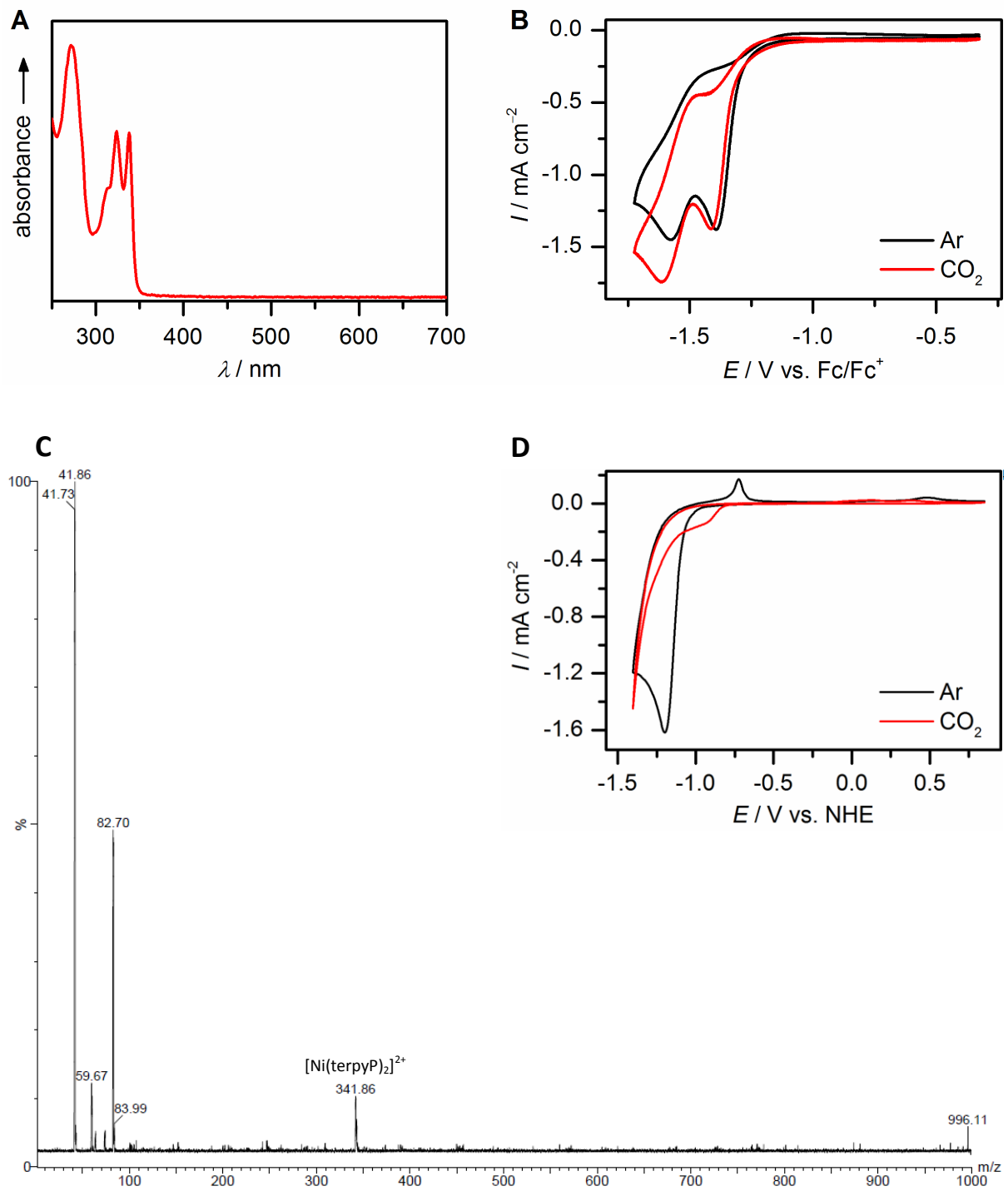

Figure S3. Characterization of self-assembled $[Ni(terpyP)_2]^{2+}$. A) UV-vis spectrum in DMF solution; B) Cyclic voltammogram (1.0 mM $Ni(BF_4)_2 \times 6H_2O$, 2.0 mM terpyP, 0.1 M $TBABF_4$ in acetonitrile/water 3:1; v = 100 mV s^{-1}, BDD working, Pt counter, Ag/AgCl reference electrode, 25°C); C) ESI-MS spectrum in acetonitrile solution; D) cyclic voltammogram (1.0 mM $Ni(BF_4)_2 \times 6H_2O$, 2.0 mM terpyP, 0.1 M TEOA, 0.1 M KCl in water/acetonitrile 19/1 v/v, pH 6.7; v = 100 mV s^{-1}, BDD working, Pt counter, Ag/AgCl reference electrode, 25°C).

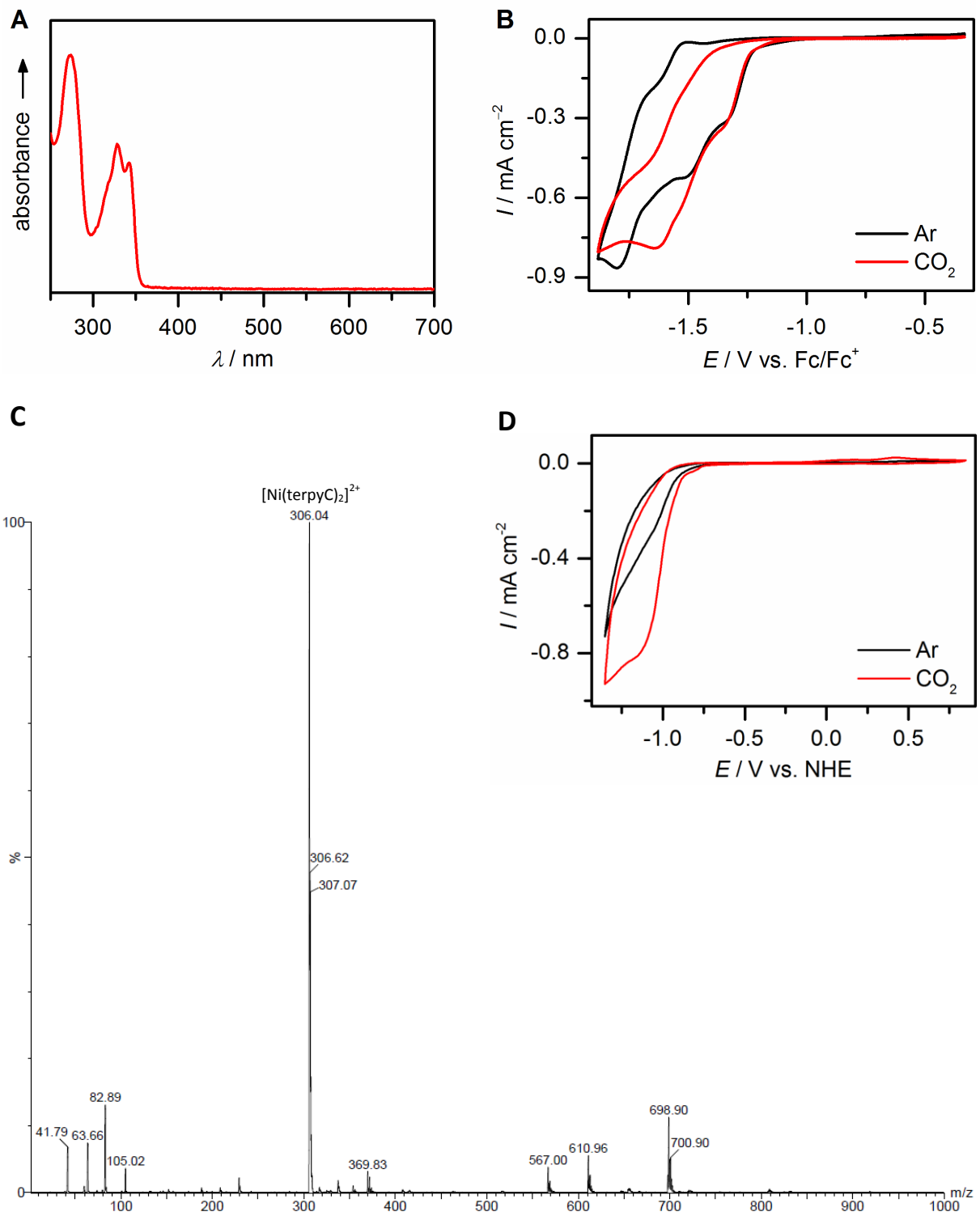

Figure S4. Characterization of self-assembled $[Ni(terpyC)_2]^{2+}$. A) UV-vis spectrum in DMF solution; B) Cyclic voltammogram (1.0 mM $Ni(BF_4)_2 \times 6H_2O$, 2.0 mM terpyC, 0.1 M $TBABF_4$ in acetonitrile/water 3:1; v = 100 mV s^{-1}, BDD working, Pt counter, Ag/AgCl reference electrode, 25°C); C) ESI-MS spectrum in acetonitrile solution; D) cyclic voltammogram (1.0 mM $Ni(BF_4)_2 \times 6H_2O$, 2.0 mM terpyC, 0.1 M TEOA, 0.1 M KCl in water/acetonitrile 19/1 v/v, pH 6.7; v = 100 mV s^{-1}, BDD working, Pt counter, Ag/AgCl reference electrode, 25°C).

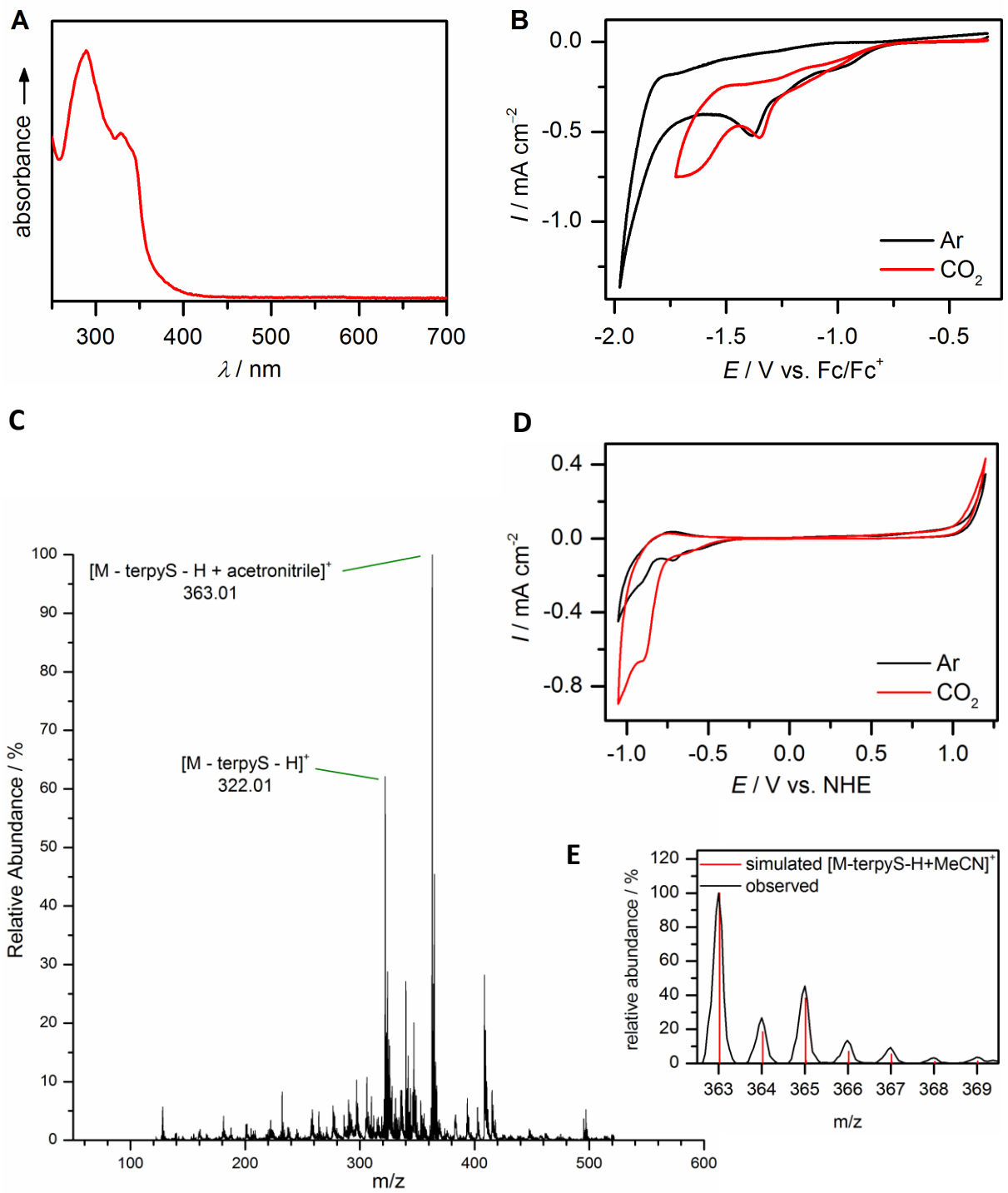

Figure S5. Characterization of self-assembled $[Ni(terpyS)_2]^{2+}$. A) UV-vis spectrum in DMF solution; B) Cyclic voltammogram (1.0 mM $Ni(BF_4)_2 \times 6H_2O$, 2.0 mM terpyS, 0.1 M $TBABF_4$ in acetonitrile/water 3:1; v = 100 mV s^{-1}, BDD working, Pt counter, Ag/AgCl reference electrode, 25°C); C) ESI-MS spectrum in acetonitrile solution (in order to achieve sufficient ionization of $[Ni(terpyS)_2]^{2+}$, the spectrum was recorded with a very high cone voltage that leads to a high signal to noise ratio); D) cyclic voltammogram (1.0 mM $Ni(BF_4)_2 \times 6H_2O$, 2.0 mM terpyS, 0.1 M TEOA, 0.1 M KCl in water/acetonitrile (19/1 v/v), pH 6.7; v = 100 mV s^{-1}, BDD working, Pt counter, Ag/AgCl reference electrode, 25°C); E) high-resolution ESI-MS spectrum in acetonitrile solution with fitting of the isotopic pattern expected for the most abundant peak.

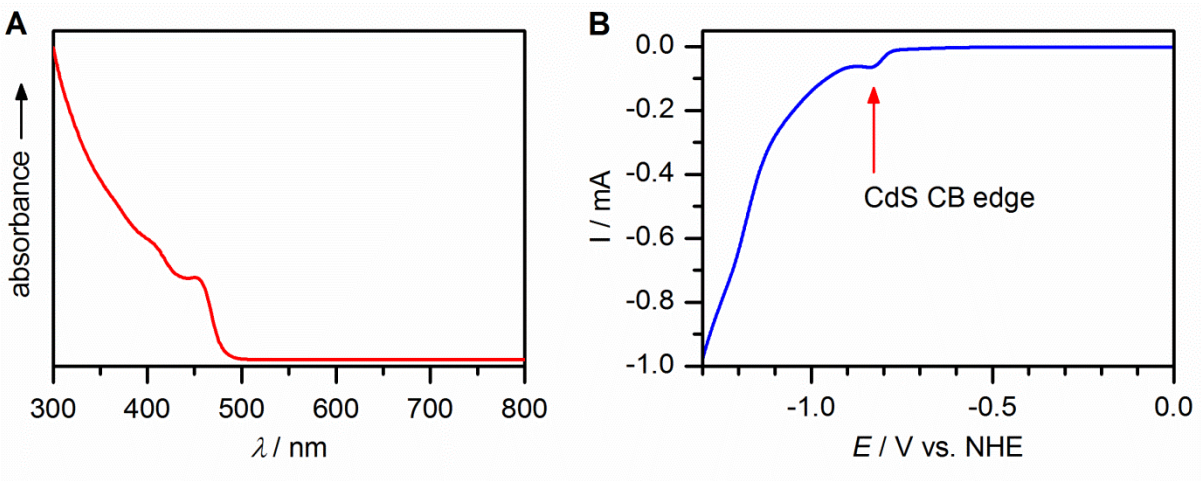

Figure S6. A) UV-vis spectrum of QD-BF_4 in DMF solution; B) Linear sweep voltammogram of QD-BF_4 immobilized on a glassy carbon electrode (0.1 M TEOA, 0.1 M KCl, pH 6.7, v = 100 mV s^{-1}, Pt counter, Ag/AgCl reference electrode, 25°C).

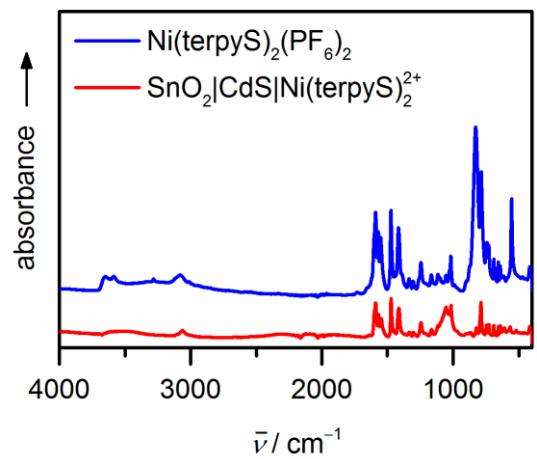

Figure S7. ATR-IR spectra of $[Ni(terpyS)]_2(PF_6)_2$ and of CdS-$[Ni(terpyS)_2]^{2+}$ immobilized on a mesoporous SnO_2 electrode.

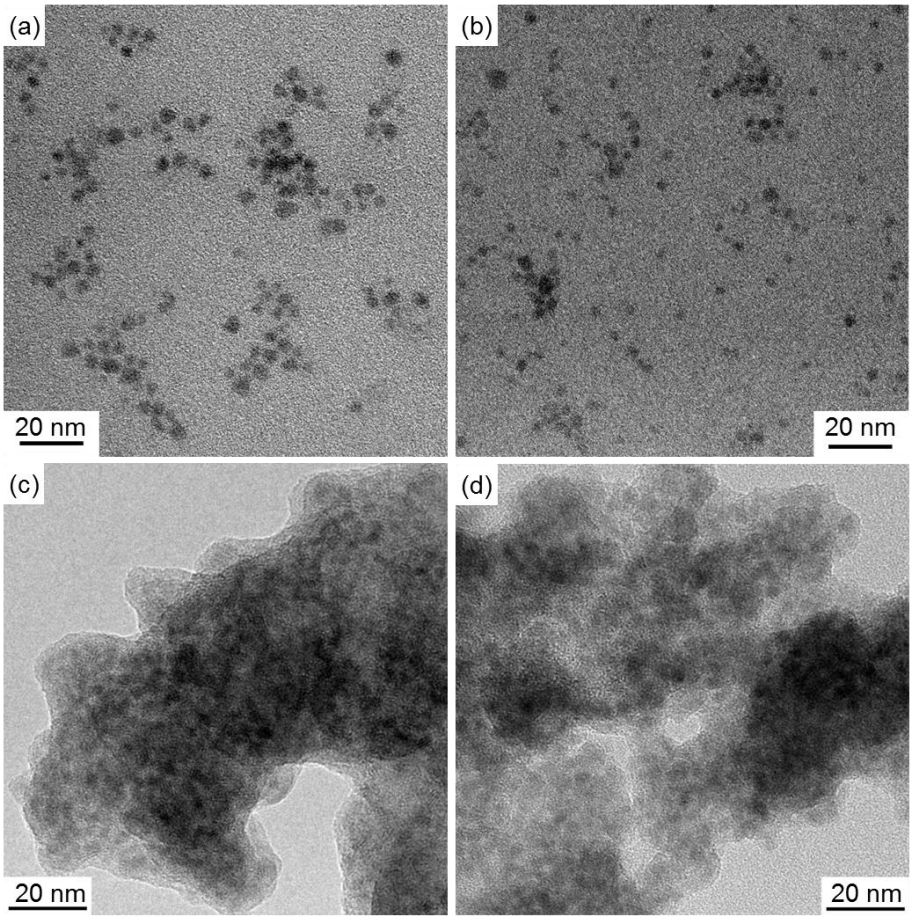

Figure S8. TEM images of CdS QDs without (a, c) and with (b, d) the addition of 100 equivalents of $[Ni(terpyS)_2]^{2+}$ in (a, b) DMF solution and (c, d) aqueous TEOA solution (0.1 M, purged with CO_2). No observable change in aggregation was induced by the addition of the catalyst.

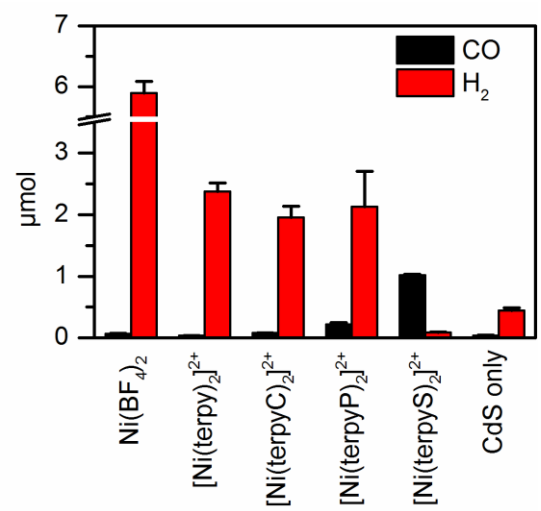

Figure S9. Product distribution during the photocatalytic CO_2 reduction using QD-BF_4 in the presence of different co-catalysts (1 μM QD-BF_4, 100 μM co-catalyst in 0.1 M aq. TEOA pH 6.7 under CO_2; 4 h irradiation, 100 mW cm^{-2}, AM1.5G, λ>400 nm, 25°C).

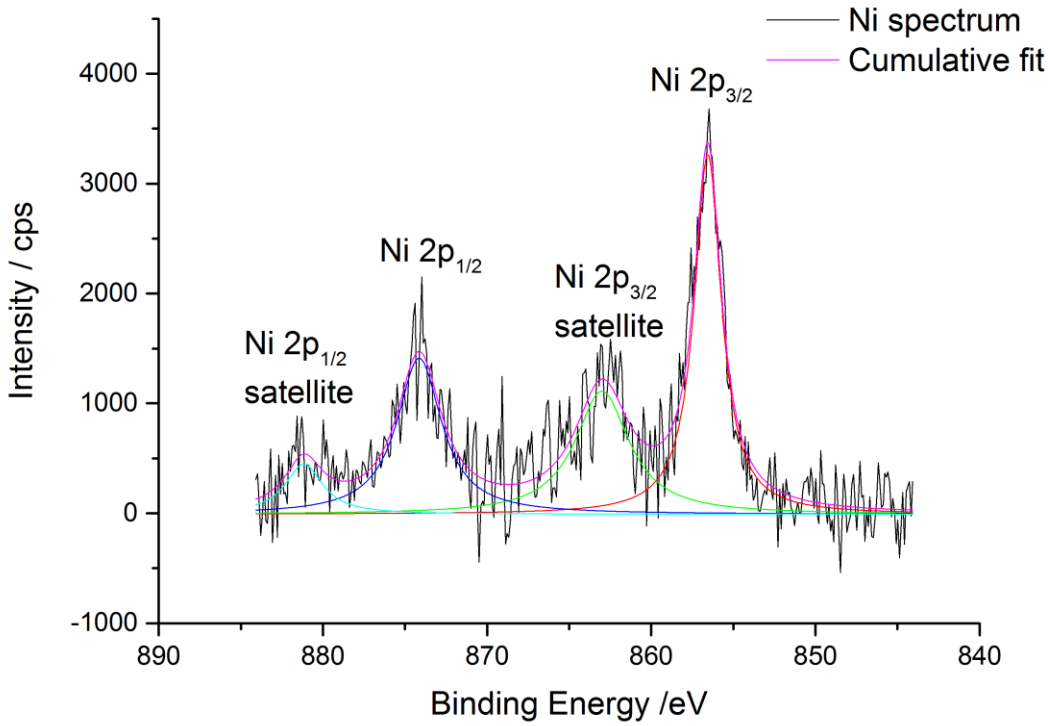

Figure S10. Ni region of the X-ray photoelectron spectrum of CdS-$[Ni(terpyS)_2]^{2+}$ hybrids after 1 h of photocatalysis (1 μM QD-BF_4, 100 μM -$[Ni(terpyS)_2]^{2+}$ in 0.1 M aq. TEOA pH 6.7 under CO_2;, 100 mW cm^{-2}, AM1.5G, λ>400 nm, 25°C).

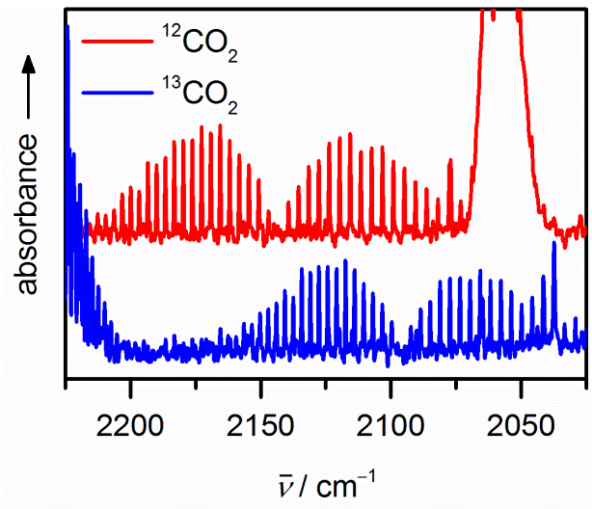

Figure S11. Gas-phase transmission IR spectra of the photocatalytic CO_2 reduction products depending on the CO_2 isotopologue starting material (1 µM QD, 100 µM $[Ni(terpyS)_2]^{2+}$ in 0.1 M TEOA under $^{12}CO_2$ or $^{13}CO_2$; 8 h irradiation, 100 mW cm^{-2}, AM1.5G, λ>400 nm, 25°C).

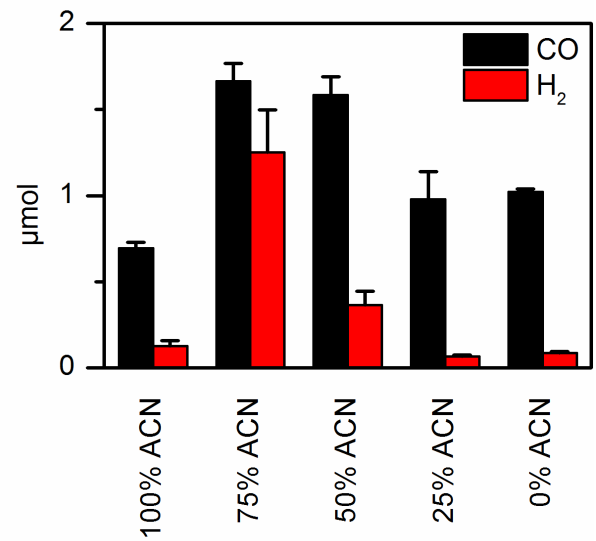

Figure S12. Product distribution during the photocatalytic CO_2 reduction using CdS-$[Ni(terpyS)_2]^{2+}$ in different H_2O/acetonitrile mixtures as solvent (1 µM QD, 100 µM $Ni(terpyS)_2^{2+}$ in 0.1 M TEOA under CO_2; 4 h irradiation, 100 mW cm^{-2}, AM1.5G, λ>400 nm, 25°C).

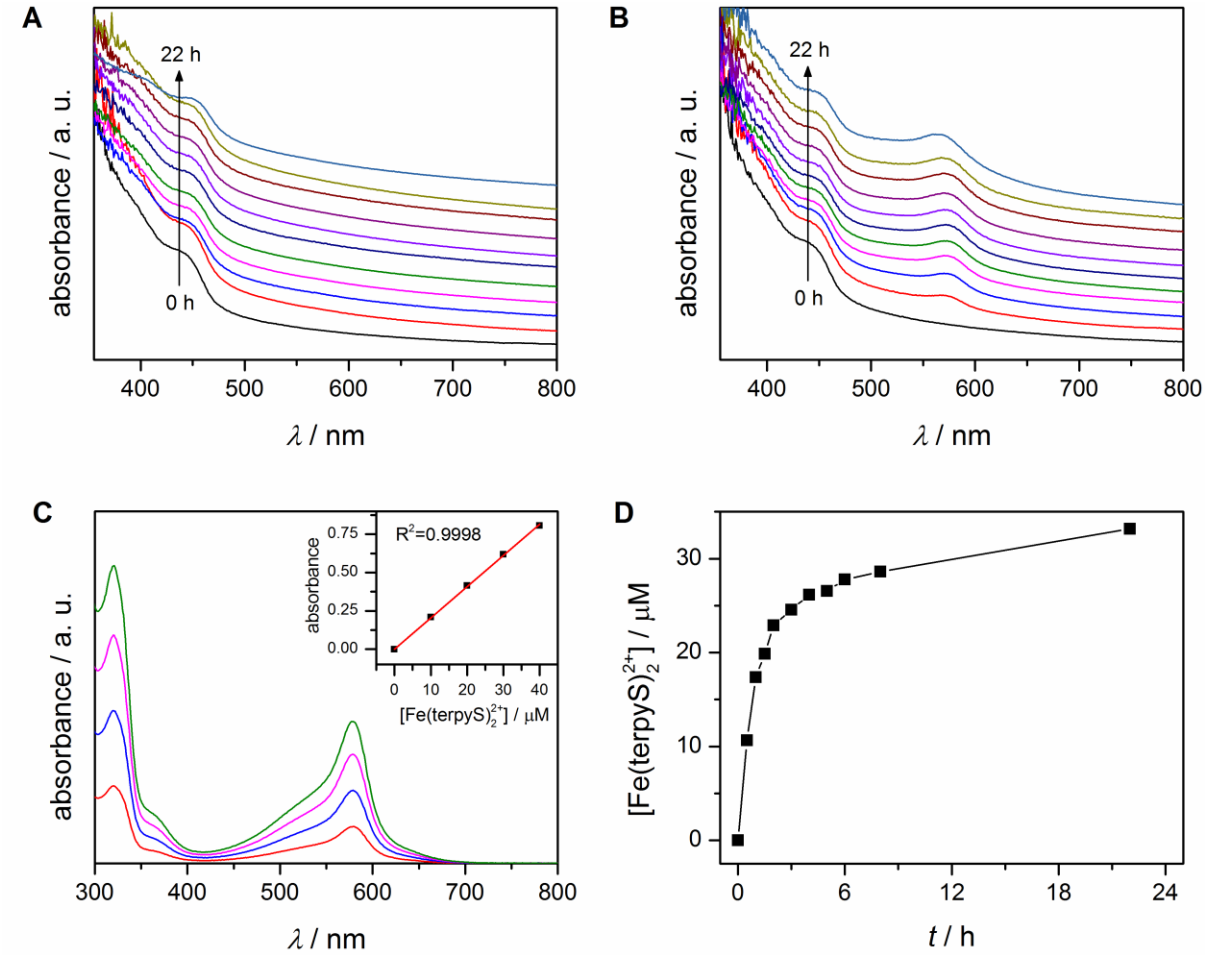

Figure S13. In-situ UV-vis spectra of the CdS-$[Ni(terpyS)_2]^{2+}$ hybrid catalyst during photocatalytic CO_2 reduction: A) Stacked spectra of CdS-$[Ni(terpyS)_2]^{2+}$ over time; B) stacked spectra of CdS-$Ni(terpyS)_2^{2+}$ in the presence of $Fe(BF_4)_2$; C) spectra of $[Fe(terpyS)_2]^{2+}$ at different concentrations and calibration curve (insert); D) concentration of $[Fe(terpyS)_2]^{2+}$ formed during catalysis in the presence of $Fe(BF_4)_2$ determined from the absorbance at 578 nm after subtraction of the initial spectrum. Conditions: 0.1 M aq. TEOA pH 6.7 under CO_2; A) 1 µM QD, 100 µM $[Ni(terpyS)_2]^{2+}$; B) 1 µM QD, 100 µM $[Ni(terpyS)_2]^{2+}$, 100 µM $Fe(BF_4)_2$), 25°C.

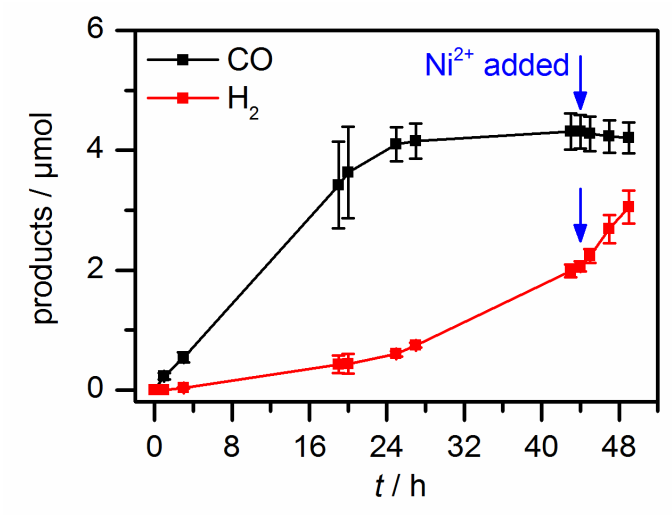

Figure S14. Long-term photocatalytic activity of CdS-$[Ni(terpyS)_2]^{2+}$ and effect of adding $Ni(BF_4)_2$ after 44 h (1 µM QD, 100 µM $[Ni(terpyS)_2]^{2+}$ in 0.1 M aq. TEOA pH 6.7 under CO_2;.5G, λ>400 nm, 25°C; after 44 hours, 200 nmol of $Ni(BF_4)_4 \times 6H_2O$ in acetonitrile was added). Note that experiments were performed with a non-calibrated solar light simulator and the intensity is therefore not precisely AM 1.5G; this resulted in a longer irradiation time required to reach full catalyst decomposition compared to Fig. 5C.

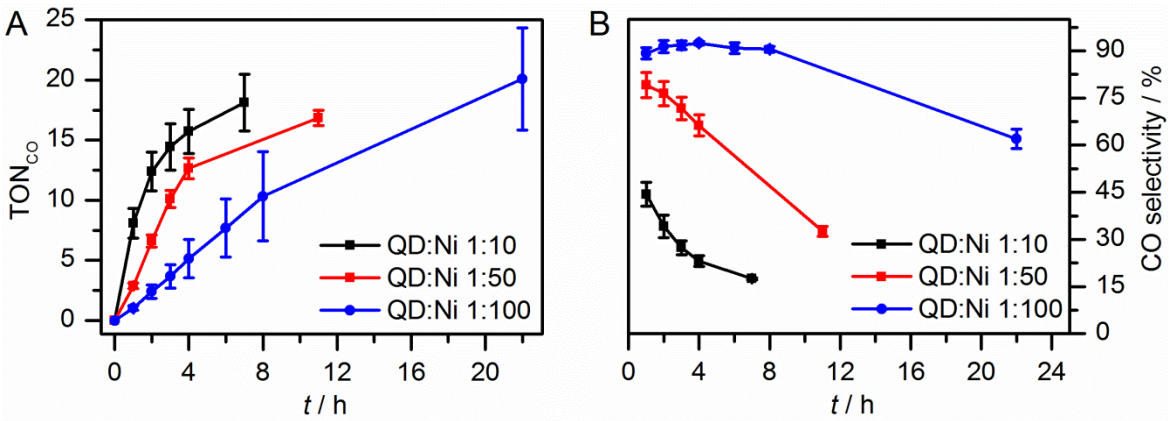

Figure S15. Photocatalytic CO_2 reduction using CdS-$[Ni(terpyS)_2]^{2+}$ in different QD:co-catalyst ratios. A) Turnover number with respect to Ni over time; B) CO vs. H_2 product selectivity over time (1 µM QD, 10/50/100 µM $[Ni(terpyS)_2]^{2+}$ in 0.1 M aq. TEOA under CO_2; 100 mW cm^{-2}, AM1.5G, λ>400 nm, 25°C).

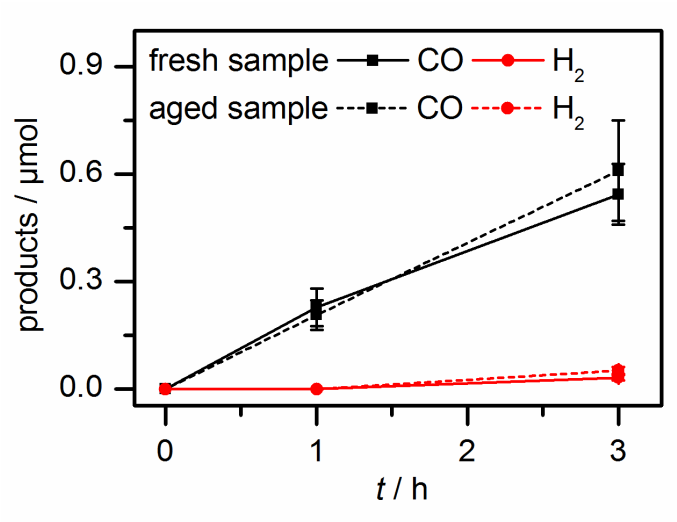

Figure S16. Effect of ageing on the photocatalytic activity of CdS-$[Ni(terpyS)_2]^{2+}$: Samples were prepared under standard conditions and used directly for photocatalytic CO_2 reduction ('fresh sample') or stirred in the dark for 22 h ('aged sample') prior to performing photocatalysis under the same conditions (1 µM QD, 100 µM $[Ni(terpyS)_2]^{2+}$ in 0.1 M aq. TEOA under CO_2; 100 mW cm^{-2}, AM1.5G, λ>400 nm, 25°C).

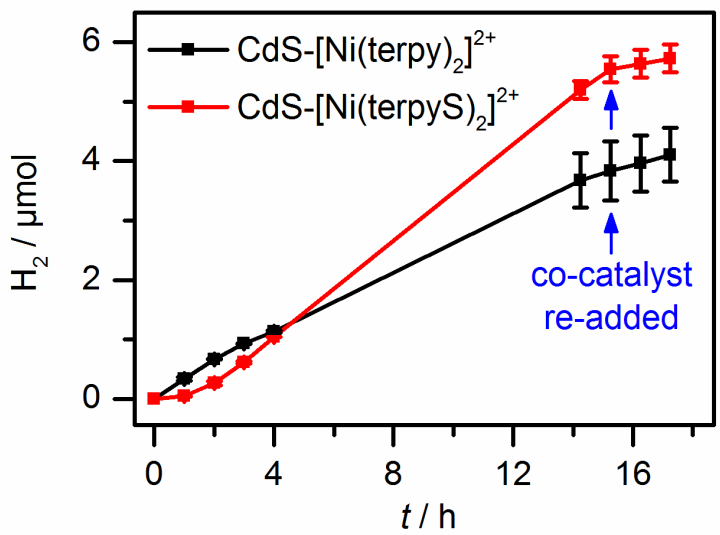

Figure S17. Photocatalytic H_2 production using CdS-$[Ni(terpy)_2]^{2+}$ and CdS-$[Ni(terpyS)_2]^{2+}$ in the absence of CO_2 (1 µM QD, 100 µM co-catalyst in 0.1 M aq. TEOA pH 6.7 under N_2; 100 mW cm^{-2}, AM1.5G, λ>400 nm, 25°C). After 15 hours, 100 nmol of co-catalyst was added and the solution was re-purged with N_2.

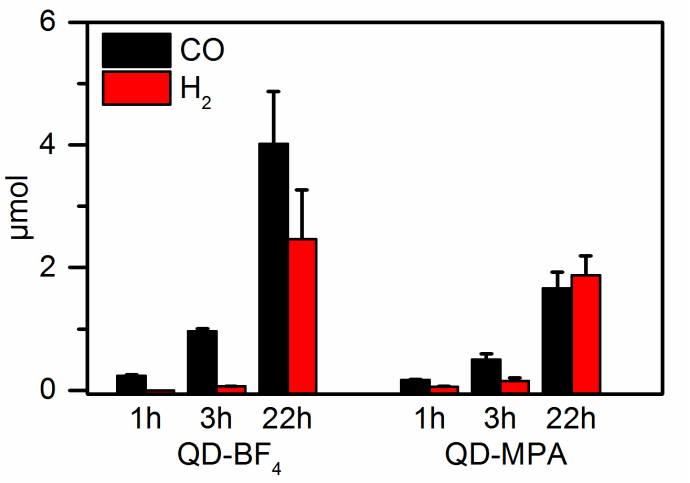

Figure S18. Product distribution during photocatalytic CO_2 reduction using different CdS quantum dots in the presence of $[Ni(terpyS)_2]^{2+}$ (1 μM QD, 100 μM $[Ni(terpyS)_2]^{2+}$ in 0.1 M aq. TEOA pH 6.7 under CO_2; 100 mW cm^{-2}, AM1.5G, λ>400 nm, 25°C).

Supporting Tables

Table S1. Electrocatalytic CO_2 reduction using self-assembled $[Ni(terpyX)_2]^{2+}$ complexes (0.25 mM $Ni(BF_4)_2 \times 6H_2O$, 0.5 mM terpyX, 0.1 M Bu_4NBF_4 in 8 mL acetonitrile/water 3:1 under CO_2; E_{appl} = –1.83 V vs. Fc/Fc^+, glassy carbon rod working, Ag/AgCl reference and Pt mesh counter electrode, rt).

time / h	n(CO) ± σ / µmol	n(H_2) ± σ / µmol	FE (CO) ± σ / %	FE (H_2) ± σ / %	TON_{Ni} (CO) ± σ	CO selectivity[a] / %
control – no catalyst						
1	0.09 ± 0.10	1.83 ± 0.81	2.0 ± 2.0	39.8 ± 12.9	-	4.62 ± 4.03
2	0.14 ± 0.14	3.85 ± 1.39	1.4 ± 1.3	36.7 ± 9.3	-	3.32 ± 2.53
3	0.17 ± 0.09	7.13 ± 3.29	0.9 ± 0.4	36.0 ± 8.5	-	2.51 ± 1.01
4	0.21 ± 0.10	10.7 ± 16.4	0.7 ± 0.3	33.9 ± 8.1	-	2.19 ± 1.01
5	0.35 ± 0.13	16.4 ± 11.5	0.8 ± 0.3	35.2 ± 11.0	-	2.52 ± 1.43
6	0.43 ± 0.12	23.0 ± 14.4	0.7 ± 0.1	35.6 ± 11.7	-	2.30 ± 1.36
12	2.42 ± 1.51	122 ± 97	0.9 ± 0.3	40.7 ± 27.6	-	3.47 ± 2.90
$[Ni(terpy)_2]^{2+}$						
1	4.86 ± 0.40	0.09 ± 0.05	33.7 ± 2.6	0.6 ±0.3	2.43 ± 0.20	98.2 ± 1.0
2	9.36 ± 1.21	1.90 ± 0.82	37.6 ± 7.2	7.5 ± 2.9	4.68 ± 0.60	82.9 ± 7.7
3	10.4 ± 0.7	4.63 ± 1.70	33.5 ± 2.1	14.7 ± 4.3	5.18 ± 0.34	69.8 ± 7.7
4	10.7 ± 0.5	8.42 ± 2.47	27.9 ± 2.3	21.6 ± 4.8	5.32 ± 0.27	56.5 ± 7.7
5	11.06 ± 0.4	12.6 ± 3.6	24.0 ± 2.3	27.1 ± 5.5	5.48 ± 0.20	47.3 ± 7.6
6	11.2 ± 0.3	17.0 ± 4.9	21.2 ± 2.3	31.4 ± 6.1	5.62 ± 0.16	40.7 ± 7.5
12	13.0 ± 0.7	42.6 ±11.5	12.8 ±1.2	41.4 ± 7.7	6.49 ± 0.36	24.1 ± 5.2
$[Ni(terpyC)_2]^{2+}$						
1	3.81 ± 0.63	1.13 ± 0.49	25.8 ±1.6	7.5 ± 2.8	1.90 ± 0.31	77.8 ± 5.3
2	7.01 ± 0.82	5.61 ± 1.91	24.0 ± 1.8	19.0 ± 5.6	3.51 ± 0.41	56.4 ± 6.2
3	9.94 ± 1.04	13.7 ± 4.1	21.5 ± 1.8	29.2 ± 6.0	4.97 ± 0.42	42.8 ± 5.7
4	12.4 ± 1.4	24.1 ± 6.7	18.8 ± 2.1	36.1 ± 6.9	6.20 ± 0.69	34.6 ± 4.4
5	14.3 ± 1.6	37.9 ± 10.7	16.2 ± 2.6	41.9 ± 7.1	7.14 ± 0.78	28.0 ± 4.0
6	15.2 ± 1.2	57.3 ± 13.9	13.4 ± 2.4	49.3 ± 5.8	7.59 ± 0.59	21.4 ± 2.9
12	17.1 ± 0.5	194 ± 59	5.40 ± 1.45	58.2 ± 8.3	8.54 ± 0.23	8.51 ± 2.19

time / h	n(CO) ± σ / µmol	n(H_2) ± σ / µmol	FE (CO) ± σ / %	FE (H_2) ± σ / %	TON_{Ni} (CO) ± σ	CO selectivity[a] / %
$[Ni(terpyP)_2]^{2+}$						
1	4.43 ± 0.79	5.69 ±0.83	28.4 ±11.5	35.9 ±11.8	2.22 ±0.40	43.7 ± 2.7
2	7.90 ± 1.85	12.1 ± 2.8	26.8 ± 10.7	40.5 ± 13.6	3.95 ± 0.93	39.6 ± 3.3
3	9.90 ± 2.91	20.9 ± 7.2	22.2 ± 9.8	45.5 ± 17.9	4.95 ± 1.45	32.8 ± 5.8
4	11.1 ± 3.6	33.1 ± 12.7	18.5 ± 9.1	52.1 ± 20.9	5.57 ± 1.81	26.3 ± 7.6
5	11.6 ± 3.7	47.5 ± 20.8	14.2 ± 6.4	53.4 ± 19.2	5.82 ± 1.85	21.5 ± 9.1
6	11.8 ± 3.3	60.2 ± 28.0	12.0 ± 4.9	55.4 ± 19.6	5.90 ± 1.63	18.6 ± 8.9
12	13.3 ± 2.5	210 ± 102	4.82 ±1.86	67.4 ± 17.7	6.63 ± 1.24	7.22 ± 4.15
$[Ni(terpyS)_2]^{2+}$						
1	3.44 ±0.77	0.14 ± 0.05	42.5 ± 5.9	1.8 ± 0.8	1.72 ± 0.38	95.8 ± 2.2
2	3.52 ± 0.82	0.26 ± 0.12	36.0 ± 5.8	2.7 ± 0.9	1.76 ± 0.41	93.0 ± 2.6
3	3.61 ± 0.79	0.46 ± 0.24	30.2 ± 2.9	3.8 ± 1.6	1.80 ± 0.39	88.7 ± 4.9
4	4.02 ± 1.31	1.68 ± 2.07	23.7 ± 1.8	8.3 ± 7.9	2.01 ± 0.66	76.4 ± 18.6
5	4.36 ± 1.73	5.23 ± 6.99	17.5 ± 3.0	15.1 ± 13.9	2.18 ± 0.87	59.5 ± 25.1
6	4.70 ± 1.81	12.1 ± 12.7	13.1 ± 3.6	25.2 ± 13.5	2.35 ± 0.92	36.7 ± 15.4
12	6.83 ± 1.29	85.6 ± 27.5	4.25 ± 1.31	51.2 ± 8.6	3.41 ± 0.65	7.58 ± 1.17

[a] CO selectivity = 100% × n(CO) / (n(CO) + n(H_2)).

Table S2. Electrocatalytic CO_2 reduction using self-assembled $[Ni(terpyX)_2]^{2+}$ complexes in aqueous solution (0.5 mM $Ni(BF_4)_2$×$6H_2O$, 1.0 mM terpyX, 0.1 M $KHCO_3$ in 8 mL water under CO_2 pH 6.7; 12 h electrolysis at E_{appl} = –0.84 V vs. NHE, glassy carbon rod working, Ag/AgCl reference and Pt mesh counter electrode, rt).

catalyst	n(CO) / µmol	n(H_2) / µmol	FE (CO) / %	FE (H_2) / %	CO selectivity[a] / %
control – no catalyst	–	0.32	–	4.2	0
$[Ni(terpy)_2]^{2+}$	0.0042	0.16	0.05	1.8	2.8
$[Ni(terpyC)_2]^{2+}$	0.19	8.0	0.43	19	2.3
$[Ni(terpyP)_2]^{2+}$	0.71	3.3	8.1	37	18
$[Ni(terpyS)_2]^{2+}$	0.071	–	3.4	–	100

[a] CO selectivity = 100% × n(CO) / (n(CO) + n(H_2)).

Table S3. Optimization of photocatalytic CO_2 reduction using self-assembled $[Ni(terpyX)_2]^{2+}$ and CdS quantum dots. Unless otherwise stated, standard conditions were: 1 µM QD, 100 µM co-catalyst, 0.1 M TEOA, 2 mL water under CO_2; 100 mW cm^{-2}, AM1.5G, λ>400 nm, 25°C).

Photocatalyst	Co-catalyst	time / h	n(CO) ± σ / µmol	n(H_2) ± σ / µmol	TON_{Ni} (CO) ± σ	CO selectivity[a] / %
varying co-catalyst						
QD-BF_4	$Ni(BF_4)_2 \times 6H_2O$	4	0.066 ± 0.007	5.89 ± 0.19	0.33 ± 0.04	1.12 ± 0.16
QD-BF_4	$[Ni(terpy)_2]^{2+}$	4	0.034 ± 0.005	2.37 ± 0.14	0.17 ± 0.02	1.42 ± 0.12
QD-BF_4	$[Ni(terpyC)_2]^{2+}$	4	0.079 ± 0.004	1.96 ± 0.18	0.40 ± 0.02	3.92 ± 0.39
QD-BF_4	$[Ni(terpyP)_2]^{2+}$	4	0.216 ± 0.033	2.13 ± 0.57	1.07 ± 0.17	10.2 ± 4.3
QD-BF_4	$[Ni(terpyS)_2]^{2+}$	4	1.02 ± 0.05	0.087 ± 0.010	5.11 ± 0.10	92.2 ± 0.7
QD-BF_4	none	4	0.039 ± 0.003	0.440 ± 0.044	-	8.14 ± 0.81
varying photocatalyst						
QD-BF_4	$[Ni(terpyS)_2]^{2+}$	3	0.96 ± 0.04	0.064 ± 0.001	4.80 ± 0.21	93.7 ± 0.4
QD-MPA	$[Ni(terpyS)_2]^{2+}$	3	0.50 ±0.09	0.15 ± 0.05	2.50 ± 0.46	75.7 ± 9.3
varying solvent						
QD-BF_4 acetonitrile	$[Ni(terpyS)_2]^{2+}$	4	0.70 ± 0.03	0.13 ± 0.03	3.48 ± 0.17	84.6 ± 3.7
QD-BF_4 acetonitrile/H_2O 3:1	$[Ni(terpyS)_2]^{2+}$	4	1.66 ± 0.10	1.25 ± 0.25	8.32 ± 0.51	57.4 ± 5.7
QD-BF_4 acetonitrile/H_2O 1:1	$[Ni(terpyS)_2]^{2+}$	4	1.58 ± 0.11	0.36 ± 0.08	7.92 ± 0.52	81.2 ± 4.4
QD-BF_4 acetonitrile/H_2O 1:3	$[Ni(terpyS)_2]^{2+}$	4	0.98 ± 0.16	0.067± 0.009	4.90 ± 0.79	93.3 ± 2.0
QD-BF_4 H_2O	$[Ni(terpyS)_2]^{2+}$	4	1.02 ± 0.05	0.087 ± 0.010	5.11 ± 0.05	92.2 ± 0.7

varying co-catalyst loading						
QD-BF_4	100 µM $[Ni(terpyS)_2]^{2+}$	1	0.209 ± 0.036	0.025 ± 0.002	1.04 ±0.18	89.2 ± 1.8
QD-BF_4	100 µM $[Ni(terpyS)_2]^{2+}$	2	0.480 ± 0.115	0.043 ± 0.003	2.40 ± 0.57	91.4 ± 1.9
QD-BF_4	100 µM $[Ni(terpyS)_2]^{2+}$	3	0.737 ± 0.195	0.064 ± 0.017	3.68 ± 0.97	91.8 ± 1.3
QD-BF_4	100 µM $[Ni(terpyS)_2]^{2+}$	4	1.03 ± 0.32	0.082 ± 0.020	5.14 ± 1.58	92.5 ± 0.6
QD-BF_4	100 µM $[Ni(terpyS)_2]^{2+}$	6	1.54 ± 0.48	0.146 ± 0.033	7.69 ± 2.41	90.9 ± 1.7
QD-BF_4	100 µM $[Ni(terpyS)_2]^{2+}$	8	2.06 ± 0.74	0.210 ± 0.039	10.3 ± 3.7	90.5 ± 0.9
QD-BF_4	100 µM $[Ni(terpyS)_2]^{2+}$	22	4.02 ± 0.85	2.46 ± 0.80	20.1 ± 4.3	62.0 ± 3.1
QD-BF_4	50 µM $[Ni(terpyS)_2]^{2+}$	1	0.290 ± 0.023	0.076 ± 0.008	2.90 ± 0.23	79.1 ± 4.0
QD-BF_4	50 µM $[Ni(terpyS)_2^{2+}$	2	0.661 ± 0.051	0.205 ± 0.016	6.61 ± 0.51	76.4 ± 3.8
QD-BF_4	50 µM $[Ni(terpyS)_2]^{2+}$	3	1.01 ± 0.07	0.399 ± 0.027	10.1 ± 0.7	71.7 ± 3.6
QD-BF_4	50 µM $[Ni(terpyS)_2]^{2+}$	4	1.26 ± 0.09	0.643 ± 0.054	12.6 ± 0.9	66.3 ± 3.3
QD-BF_4	50 µM $[Ni(terpyS)_2]^{2+}$	11	1.68 ± 0.06	3.49 ± 0.34	16.8 ± 0.6	32.6 ± 1.6
QD-BF_4	10 µM $[Ni(terpyS)_2]^{2+}$	1	0.162 ± 0.025	0.202 ± 0.020	8.09 ± 1.2	44.3 ± 3.8
QD-BF_4	10 µM $[Ni(terpyS)_2]^{2+}$	2	0.248 ± 0.032	0.479 ± 0.061	12.4 ± 1.6	34.2 ± 3.6
QD-BF_4	10 µM $[Ni(terpyS)_2]^{2+}$	3	0.289 ± 0.039	0.766 ± 0.069	14.4 ± 1.9	27.3 ± 2.2
QD-BF_4	10 µM $[Ni(terpyS)_2]^{2+}$	4	0.314 ± 0.038	1.04 ± 0.080	15.7 ± 1.8	23.2 ± 1.4
QD-BF_4	10 µM $[Ni(terpyS)_2]^{2+}$	7	0.363 ± 0.047	1.71 ± 0.19	18.1 ± 2.6	17.5 ± 0.4
varying irradiation spectrum						
QD-BF_4 λ > 400 nm	$[Ni(terpyS)_2]^{2+}$	4	1.02 ± 0.05	0.087 ± 0.010	5.11 ± 0.10	92.2 ± 0.7
QD-BF_4 full spectrum AM1.5	$[Ni(terpyS)_2]^{2+}$	4	1.24 ± 0.17	0.068 ± 0.017	6.22 ± 0.87	94.7 ± 0.4

[a] CO selectivity = 100% × n(CO) / (n(CO) + n(H_2)).

Table S4. Catalyst attachment during photocatalytic CO_2 reduction using self-assembled $[Ni(terpyS)_2]^{2+}$, $[Ni(terpy)_2]^{2+}$, or $Ni(BF_4)_2$ and CdS quantum dots based on ion-coupled plasma optical emission spectroscopy (ICP-OES; 1 µM QD-BF_4, 100 µM Ni^{2+}, in 2 mL 0.1 M aq. TEOA under CO_2; 100 mW cm^{-2}, AM1.5G, λ>400 nm, 25°C).

Catalyst	time / h	Ni / nmol	Cd / µmol	QD-BF_4 / nmol	Ni per QD / mol Ni (mol QD)$^{-1}$
$[Ni(terpyS)_2]^{2+}$[a]	0	71.0 ± 1.6	1.96 ± 0.17	1.23 ± 0.15	58.6 ± 8.2
	1	73.2 ± 0.8	2.16 ± 0.11	1.38 ± 0.07	53.2 ± 2.0
	6	47.1 ± 8.9	2.14 ± 0.11	1.10 ± 0.35	44.9 ± 6.2
	22	5.6 ± 1.2	2.06 ± 0.01	1.30 ± 0.01	4.3 ± 0.9
$[Ni(terpy)_2]^{2+}$[b]	1	6.1	1.87	1.18	5.2
$Ni(BF_4)_2$[b]	1	5.0	1.06	0.67	7.5

[a] Average of two independent measurements
[b] Single measurement

Table S5. Photocatalytic proton reduction using self-assembled $[Ni(terpyX)_2]^{2+}$ and CdS quantum dots in the absence of CO_2 (1 µM QD, 100 µM co-catalyst, 0.1 M TEOA, 2 mL water pH6.7 under N_2; 100 mW cm^{-2}, AM1.5G, λ>400 nm, 25°C). Data is from two independent experiments.

	$[Ni(terpy)_2]^{2+}$	$[Ni(terpyS)_2]^{2+}$
time / h	$n(H_2) \pm \sigma$ / µmol	$n(H_2) \pm \sigma$ / µmol
1	0.338 ± 0.031	0.047 ± 0.006
2	0.670 ± 0.067	0.264 ± 0.034
3	0.931 ± 0.004	0.612 ± 0.031
4	1.13 ± 0.02	1.05 ± 0.05
14	3.68 ± 0.46	5.20 ± 0.15
15	3.84 ± 0.50	5.55 ± 0.22
100 nmols co-catalyst added, solution re-purged with N_2		
16	0.123 ± 0.023	0.092 ± 0.013
17	0.270 ± 0.040	0.183 ± 0.015

Table S6. External quantum efficiency (EQE) determination for the photocatalytic CO_2 reduction using self-assembled $[Ni(terpyS)_2]^{2+}$ and CdS quantum dots (1 µM QD-BF_4, 100 µM $[Ni(terpyS)_2]^{2+}$, in 2 mL 0.1 M aq. TEOA under CO_2; I = 1.55 mW cm^{-2}, A=0.28 cm^2, λ=400±5 nm, rt).

time / h	n(CO) / µmol[a]	EQY_{CO} / %[b]
3	0.009 ± 0.003	0.13 ± 0.04
4	0.016 ± 0.004	0.31 ± 0.07
6	0.025 ± 0.004	0.26 ± 0.12
7	0.032 ± 0.005	0.23 ± 0.02
8	0.043 ± 0.001	0.30 ± 0.01

[a] Cumulative CO measured in headspace.
[b] Quantum efficiency measured per hour.

Supporting references

(1) Arana, C.; Yan, S.; Keshavarz-K, M.; Potts, K. T.; Abruna, H. D. *Inorg. Chem.* **1992**, *31*, 3680-3682.

(2) (a) Chang, C. M.; Orchard, K. L.; Martindale, B. C. M.; Reisner, E. *J. Mater. Chem. A* **2016**, *4*, 2856-2862; (b) Kuehnel, M. F.; Wakerley, D. W.; Orchard, K. L.; Reisner, E. *Angew. Chem. Int. Ed.* **2015**, *54*, 9627-9631.

(3) Huang, L.; Wang, X.; Yang, J.; Liu, G.; Han, J.; Li, C. *J. Phys. Chem. C* **2013**, *117*, 11584-11591.

(4) Rosen, E. L.; Buonsanti, R.; Llordes, A.; Sawvel, A. M.; Milliron, D. J.; Helms, B. A. *Angew. Chem. Int. Ed.* **2012**, *51*, 684-689.

(5) Aldana, J.; Lavelle, N.; Wang, Y.; Peng, X. *J. Am. Chem. Soc.* **2005**, *127*, 2496-2504.

(6) Yu, W. W.; Qu, L.; Guo, W.; Peng, X. *Chem. Mater.* **2003**, *15*, 2854-2860.

(7) Simon, T.; Bouchonville, N.; Berr, M. J.; Vaneski, A.; Adrović, A.; Volbers, D.; Wyrwich, R.; Döblinger, M.; Susha, A. S.; Rogach, A. L.; Jäckel, F.; Stolarczyk, J. K.; Feldmann, J. *Nat. Mater.* **2014**, *13*, 1013-1018.

(8) Muresan, N. M.; Willkomm, J.; Mersch, D.; Vaynzof, Y.; Reisner, E. *Angew. Chem. Int. Ed.* **2012**, *51*, 12749-12753.

End of Supporting Information